A numerical study into the influence of quantum dot size on the sub-bandgap interband photocurrent in intermediate band solar cells

Alexander Mellor, Antonio Luque, Ignacio Tobías, and Antonio Martí

Citation: AIP Advances **3**, 022116 (2013); doi: 10.1063/1.4792598

View online: http://dx.doi.org/10.1063/1.4792598

View Table of Contents: http://aipadvances.aip.org/resource/1/AAIDBI/v3/i2

Published by the American Institute of Physics.

AIP ADVANCES **3**, 022116 (2013)

A numerical study into the influence of quantum dot size on the sub-bandgap interband photocurrent in intermediate band solar cells

Alexander Mellor, Antonio Luque, Ignacio Tobías, and Antonio Martí
Instituto de Energía Solar, Universidad Politécnica de Madrid, 28040 Madrid, Spain

(Received 8 November 2012; accepted 4 February 2013; published online 8 February 2013)

A numerical study is presented of the sub-bandgap interband photon absorption in quantum dot intermediate band solar cells. Absorption coefficients and photocurrent densities are calculated for the valence band to intermediate band transitions using a four-band k · p method. It is found that reducing the quantum dot width in the plane perpendicular to the growth direction increases the photocurrent from the valence band to the intermediate-band ground state if the fractional surface coverage of quantum dots is conserved. This provides a path to increase the sub-bandgap photocurrent in intermediate band solar cells. *Copyright 2013 Author(s). This article is distributed under a Creative Commons Attribution 3.0 Unported License*. [http://dx.doi.org/10.1063/1.4792598]

I. INTRODUCTION

The intermediate band solar cell (IBSC) is a high efficiency solar cell concept whose detailed balance efficiency limit has been calculated as 63%,[1] to be compared to the Schockly-Queisser limit of 41%[2] for conventional single-bandgap solar cells (both values have been calculated assuming maximum light concentration and treating the sun as a blackbody at 6000 K). The concept is based on the introduction of an intermediate band (IB) between the valence band (VB) and conduction band (CB) of a semiconductor. The IB allows an increase in photocurrent via a two sub-bandgap photon absorption process in which one photon promotes an electron from the VB to the IB and another promotes an electron from the IB to the CB, creating a single electron-hole pair.

IBSCs have been realized in which the IB is constituted by the ground state energy levels of InAs quantum dots (QDs) in a GaAs matrix.[3–8] The bandgaps of this system are not optimal, but it has allowed the basic principles of IB operation to be proven.[9,10] These devices suffer from weak sub-bandgap absorption.[11,12]

In previous works, a model was presented for the numerical study of the intraband (IB-CB)[13,14] and interband (VB-IB)[15,16] transitions in InAs/GaAs QDs, providing a formula for calculating bound state energy levels and absorption coefficients. In a recent letter, this model was applied to studying the effect of decreasing the QD size on the IB energy levels and IB-CB photocurrent.[17] It was argued that reducing the width from 16 nm to 10 nm could be desirable in two respects. Firstly, at this QD width, all excited states are removed from the forbidden band of the matrix material. Recent calculations[18] have shown that the presence of these excited states is responsible for the measured[12] carrier escape between the IB and the CB. This carrier escape ultimately inhibits the splitting of the IB and CB quasi Fermi levels and thus prevents QD-IBSCs from simultaneously achieving high sub-bandgap photocurrents and high open circuit voltages[11] (it should be noted that high open circuit voltages have been achieved in similar systems by some authors,[8] but not simultaneously with strong sub-bandgap absorption). Secondly, the IB-CB photocurrent was predicted to be significantly increased for a width of 10 nm as opposed to 16 nm.

In this work, we complete the picture by studying the effect of reducing the QD size on the VB-IB absorption coefficients and photocurrent. As before, we take as a benchmark the QD parameters of the fabricated QD-IBSC presented and characterised in,[12,19] in which it is named SB and S3 respectively.

This system consisted of a 30-layer stack of In(Ga)As/GaAs QDs, with a surface density of 4×10^{10} cm^{-2}, grown on a GaAs substrate. The QDs had the shape of truncated quadrangular pyramids with dimensions of $16 \times 16 \times 6$ nm^3. These have been modelled as square based parallelepipeds in this and the aforementioned numerical studies. All calculations performed in this work are based on this QD layer stack and the only parameters varied are the QD dimensions. Further details of the growth conditions of reals samples can be found in the aforementioned references.

II. CALCULATION METHOD

The calculations made in this work employ a multi-band k · p method.[20] The eigenstate wavefunctions are expressed as

$$\Xi(\mathbf{r}) = \sum_{v} u_{v,0}(\mathbf{r})\,\Psi_v(\mathbf{r}) \tag{1}$$

where v is the band index and $u_{v,0}(\boldsymbol{r})$ are the involutes, which are the exact solutions of the time-independent Schrödinger equation at the Γ point ($\boldsymbol{k} = 0$) for the zincblende crystal structure in the absence of the QD. $\Psi_v(\mathbf{r}, t)$ is the envelope function, which is found by solution of the multiband effective mass equation

$$\sum_{v} H_{vv'}(-i\nabla)\,\Psi_v(\mathbf{r}) + U(\mathbf{r})\,\Psi_v(\mathbf{r}) = E\Psi_v(\mathbf{r}) \tag{2}$$

where E is the energy eigenvalue and $U(\mathbf{r})$ is the mesoscopically varying potential: that caused by the QD. The periodically varying part of the potential is accounted for in the Hamiltonian $H_{vv'}$.This analytical Hamiltonian can be found in the literature.[20]

In our model, we consider four bands: the conduction band (cb), light-hole band (lh), heavy-hole band (hh) and split-off band (so), the latter three constituting the valence band (VB). In each band, each state is doubly degenerated with up and down spin. The analytical Hamiltonian, when truncated in the four-band approximation, produces energy eigenvalues that are inconsistent with experimental data. We therefore employ a modified empirical Hamiltonian, whose eigenvalues are determined by the experimental effective masses (in substitution of the more commonly used Luttinger parameters), but whose eigenvectors are the same as those of the analytical Hamiltonian. In doing so, we implicitly take into account spin-orbit coupling effects that were ignored in our choice of the analytical Hamiltonian. This empirical Hamiltonian was first presented in Ref. 15 and further modified in Ref. 16 to take account of symmetry considerations; we use the Hamiltonian found in the latter reference. The Hamiltonian is diagonalized so that Equation (2) becomes four decoupled equations; one for each band.

The QD is modelled as a square-based parallelepiped of width a_x and height a_z (z is normal to the solar-cell faces and parallel to the growth direction of the QDs). $U(r)$ is modelled as a square potential well for the CB and a square potential pedestal for the VB bands (lh, hh and so). Under these conditions, Equation (2) is solved using a separation of the x, y and z variables yielding solutions for the envelope functions that are indexed by the band index v (cb, lh, hh and so) and three quantum numbers (n_x, n_y, n_z), these being respectively the index of the constituting one-dimensional functions in the x, y and z variables. Each solution is projected back onto the involutes using the transformation matrix used to make the diagonalization (for details, see Refs. 15 and 16).

The absorption coefficient for a photon absorption in a transition between two states i and j is

$$\alpha_{i\to j} = \frac{2\pi^2 q_e^2}{nch\varepsilon_0}\frac{FN_l}{4a_x^2}|\langle\Xi_i|\mathbf{r}\cdot\boldsymbol{\varepsilon}|\Xi_j\rangle|^2 f_i(1-f_j) \tag{3}$$

where n is the refractive index of the medium (taken to be that of the GaAs matrix), f and f' are the Fermi factors respectively describing the probability of occupation of the initial and final states, ε is the unit polarization vector of the photon, F is the fractional coverage of the xy plane with QDs and N_l is the number of QD layers per unit length in the z direction. All other symbols have their usual definitions or have been defined previously. In this work, as the QD width a_x is varied, F and N_l assume fixed values of 0.1 and 125 000 cm^{-1} respectively; these being the measured values in

Refs. 12 and 19. This implies that, as the width is reduced, the volume density of QDs remains fixed and the number density of QDs increases as $1/a^2$.We assume unpolarized normally incident light; thus, we take the time average of x and y polarizations such that

$$|\langle \Xi|\mathbf{r}\cdot\varepsilon|\Xi'\rangle|^2 = \frac{1}{2}|\langle \Xi|\mathrm{x}|\Xi'\rangle|^2 + \frac{1}{2}|\langle \Xi|\mathrm{y}|\Xi'\rangle|^2 \tag{4}$$

The band edge offsets between the GaAs matrix and InAs QD are taken to be 0.473 eV in the CB, 0.210 eV in the hh and lh bands and 0.339 eV in the so band. The band gap of GaAs is taken to be 1.42 eV.

It should be noted that this model is simpler than others that appear in the Literature.[15,21] It allows us to perform parameter sweeps without the need for large computing capacity, as is done in this work. The method has been used to model the QD array presented in Refs. 12 and 19 has reproduced the measured internal quantum efficiency with good accuracy.[15,16] We consider this good agreement to be a confirmation of its efficacy.

In previous numerical studies, it has been assumed that all VB states have a Fermi factor $f = 1$, the IB ground state has $f = 0.5$ and all other IB states and CB states have $f = 0$. In this study, we prefer to make no comment on the occupancy of the states and instead define the quantity α^{max} such that

$$\alpha_{i\to j} := \alpha^{max}_{i\to j} f_i(1 - f_j) \tag{5}$$

α^{max} represents the strength of the transition, which can later be modified by the occupancies. It is the quantity that would be the starting point for a realistic detailed balance study.[18]

III. RESULTS AND DISCUSSION

Figure 1(a) (left) shows a simplified spatial band diagram for a $16 \times 16 \times 6$ nm^3 QD with the other relevant parameters as defined above. Horizontal lines represent confined state energy levels: blue for conduction band (CB) states, magenta for heavy holes (hh), red for light holes (lh) and green for split-off band (so) states. Within the CB potential well, there are three distinct bound-state energy levels, which are separated from the rest of the CB states. Within this study, these are referred to as IB states (although it should be noted that they are CB states modified by the presence of the QD). The bound states whose energy is above the matrix CB band edge (so-called virtual bound states (VBSs)) are here considered part of the device CB. The VB potential pedestal contains a near continuum of hh states, due to their high effective mass. Due to the close packing of these states, they are considered not as a separate band but as an extension of the device VB into the forbidden band. Note that some CB and so VBSs that extend deep into the respective bands are not shown in this figure or in later figures. Note that IB(2,1,1) actually refers to the degenerate pair IB(2,1,1)/IB(1,2,1).

We are interested in the net contribution of transitions from all VB (hh, lh and so) states to each individual IB state. An absorption coefficient has been calculated for each final IB state by

$$\alpha^{max}_{VB\to j} = \sum_{i\varepsilon\ all\ VB\ states} \alpha^{max}_{i\to j} \tag{6}$$

where i denotes the initial and j the final state. The absorption coefficients are plotted in Figure 1(a) (right) for all final IB states. Although in each case the absorption coefficient sums contributions from the 169 VB states, distinct peaks can be seen pertaining to a few dominant transitions. Taking $\alpha^{max}_{VB\to \mathrm{IB}(1,1,1)}$ as an example, the dominant transitions are those from the hh (1,1,1), hh(4,1,1), hh(6,1,1) and lh (2,1,1) states (the latter three have degenerate counterparts hh(1,4,1), hh(1,6,1) and lh (1,2,1), which make an equal contribution). Each peak in the absorption curve is labelled with the corresponding initial state and these transitions are shown as black arrows in Figure 1(a) (left). The shown $\alpha^{max}_{VB\to \mathrm{IB}(2,1,1)}$ is actually the sum of the absorption coefficients for the degenerate final states IB(2,1,1) and IB(1,2,1). This absorption coefficient is larger than the others due to this degeneracy. An absorption coefficient has also been calculated for the sum of the bound-state VB to bound-state

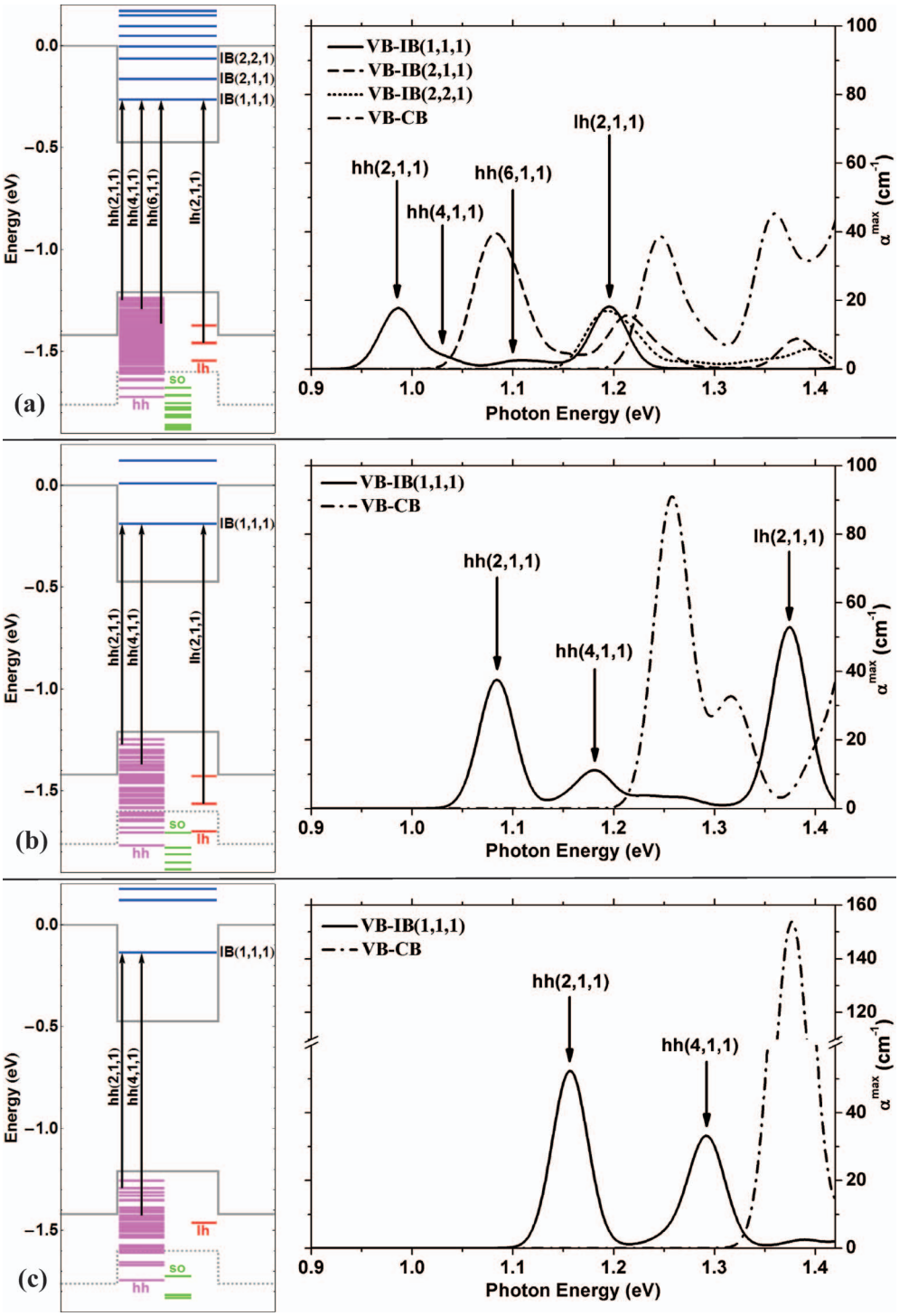

FIG. 1. Results for QD dimensions of (a) $16 \times 16 \times 6$ nm^3, (b) $10 \times 10 \times 6$ nm^3, (c) $8 \times 8 \times 6$ nm^3. Left: Band diagrams showing the band offsets and bound state energy levels. The CB, hh and lh band edges are shown as solid grey lines (the hh and lh band edges coincide). The so band edge is shown as a dashed grey line. Arrows denote the dominant transitions whose final state is the IB(1,1,1) state. These arrows are labelled with the initial state of the transition. Right: absorption coefficients (as defined in Equations (5) and (6)) for the net transitions from all VB states to a single IB state. The final IB state for each curve is shown in the figure legends. Peaks in the VB-IB(1,1,1) absorption coefficient are labelled with their initial state in the VB; these labels correspond to the arrows in the left figures. The absorption coefficient for bound-bound VB-CB transitions is also shown as defined in Equation (7). The absorption plots include photon energies up to the GaAs bandgap. Photons with greater energy are assumed to be absorbed by the emitter before reaching the QD stack.

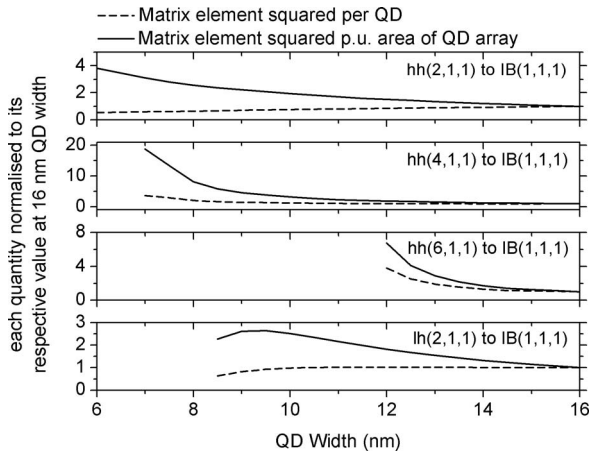

FIG. 2. Dashed curves: matrix element squared per QD ($\langle \Xi | \mathbf{r} \cdot \varepsilon | \Xi' \rangle^2$). Solid curves: matrix element squared per unit area of QD array ($\langle \Xi | \mathbf{r} \cdot \varepsilon | \Xi' \rangle^2 a_x^{-2}$). From top to bottom, the initial states of the transition are hh(2,1,1), hh(4,1,1), hh(6,1,1) and lh(2,1,1). The final state is IB(1,1,1) in all cases. Each quantity has been normalised by the value it takes for a QD width of 16 nm. The QD height is kept constant at 6 nm.

CB transitions by

$$\alpha^{max}_{VB \to CB} = \sum_{j \, \varepsilon \, all \; CB \; states} \alpha^{max}_{VB \to j} \tag{7}$$

where the sum over CB states does not include the IB states. This is also shown in the figure.

The calculations have been repeated for a $10 \times 10 \times 6$ nm^3 QD ($a_x = 10$ nm) and for an $8 \times 8 \times 6$ nm^3 QD ($a_x = 8$ nm). The results are shown in Figure 1(b) and 1(c). Note that Figure 1(c) has a break in the y scale to allow all graphs to be plotted with the same scaling. For these dimensions, there is only a single IB energy level. This result has been presented in previous work concerning the IB-CB transitions and the possible benefits of such a configuration are discussed therein.[17] Regarding the VB-IB transitions, some further observations can be made. Firstly, there is a general increase in the absorption coefficient on decreasing the QD width. This is discussed in the following paragraph. Secondly, the absorption peaks move to higher energy due to the bound states moving deeper into their respective bands. This is most pronounced for the transition whose initial state is lh(2,1,1). Finally, for the $10 \times 10 \times 6$ nm^3 QD, the hh(6,1,1) absorption peak is no longer present, and, for the $8 \times 8 \times 6$ nm^3 QD, the lh(2,1,1) absorption peak is no longer present. This is due to the disappearance of the respective states in the VB at these QD widths. This will have some negative effect on the overall VB-IB photocurrent, as shall be seen later in this letter.

It was observed in the previous paragraph that there is a tendency for the absorption coefficient to increase with decreasing QD width. This is similar to a result presented in previous work[17] for the IB-CB transition. Both results require some qualification. The results have been obtained under the assumption that the fractional coverage of the growth plane with QDs remains a constant $F = 0.1$. This implies that the number of QDs per unit area (and volume) changes as a_x^{-2}. Hence a lower QD width implies more QDs. In Figure 2, we show, for certain important transitions, the matrix element $|\langle \Xi | \mathbf{r} \cdot \varepsilon | \Xi' \rangle|^2$ (dashed curves) and the matrix element divided by the QD area in the growth plane $|\langle \Xi | \mathbf{r} \cdot \varepsilon | \Xi' \rangle|^2 a_x^{-2}$ (solid curves). The former is proportional to the transition strength per QD and the latter is proportional to the transition strength per unit area of the QD array. Each quantity is normalised to the value it takes for a QD width of 16 nm. It can be seen that the transition strength per dot can either increase or decrease as a function of the QD width, depending on the transition. However, in no case does the transition strength decrease faster than a_x^2 on decreasing the QD size, hence the obtained result.

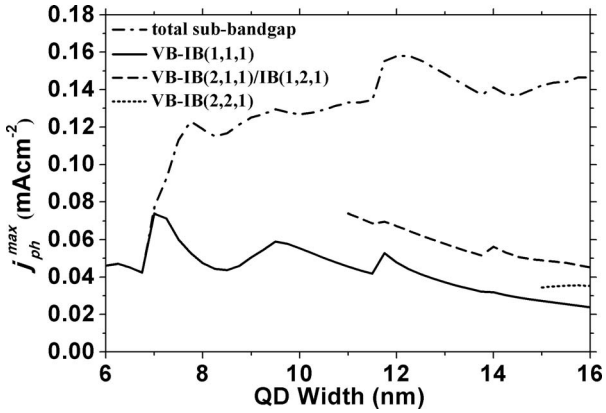

FIG. 3. the net absorbed photocurrent density for transitions from all VB states to a single IB state as a function of the QD width. The final IB state for each curve is specified in the figure legend. Also plotted is the total sub-bandgap absorbed photocurrent density, which is the sum of all interband transitions from VB states to IB and CB states. Only transitions excited by photons below the GaAs bandgap energy are consider in all cases. The QD height is kept constant at 6 nm.

For each final IB state, an absorbed photocurrent density has been calculated by

$$j_{ph,VB\to \mathrm{j}}^{max} = \int_{E<1.42\,eV} q_e \Phi_{BB,T_S} \left(1 - \exp\left(-\alpha_{VB\to j}^{max} W\right)\right) dE \tag{8}$$

where $W = 2.4\ \mu$m is thickness of the QD stack (corresponding the aforementioned 30 layer stack detailed in Refs. 12,19) and Φ_{BB,T_S} is the photon flux incident from the sun, modelled to be blackbody radiation at 5762 K without concentration (if concentration were included, the calculated current density would simply increase linearly with increased concentration factor under the assumptions of the model). A cut-off energy of 1.42 eV (the band gap energy of GaAs) is used because all photons with greater energy are assumed to be absorbed in the GaAs layer that is above the QD stack. The superscript *max* denotes that this is the value without correction for the occupancies of each state; this value therefore represents a maximum. Usually the occupancy of the IB(1,1,1) state causes the current it absorbs to be reduced by half, whereas no reduction is expected for the other states.

$j_{ph,VB\to \mathrm{j}}^{max}$ is plotted for all final IB states as a function of the QD width in Figure 3. For smaller QDs, the IB(2,1,1) and IB(2,2,1) states are pushed into the matrix CB energy range and cease to be IB states; hence, these curves do no continue over the whole range. Also plotted is the total sub-bandgap j_{ph}^{max}, which is the sum of all interband transitions from the VB that are below the cut-off energy (note that, since the VB potential pedestal extends into the forbidden band, this includes not only transitions to IB states but also to some CB states). The tendency is for the total sub-bandgap absorbed photocurrent to decrease with decreasing QD width. This is due to the energy of the constituent transitions being pushed above the cut-off energy. However, for the individual IB(1,1,1) and IB(2,1,1) final states, there is a tendency for the photocurrent density to increase on decreasing the QD width as a result of the increasing magnitude of the absorption coefficients. Looking at $j_{ph,VB\to \mathrm{IB(1,1,1)}}^{max}$, there are sharp drops in the curve going from right to left. These each correspond to an initial state that has ceased to exist. The drops at widths of 12, 9 and 7 nm correspond to the disappearance of the hh(6,1,1), lh(2,1,1) and hh(4,1,1) states respectively. In our previous work, the $10 \times 10 \times 6$ nm^3 QD was identified as being promising from a viewpoint of IB energy levels and IB-CB photocurrent. Figure 3 suggests it may be a promising candidate from a viewpoint of VB-IB photocurrent as well. Of course such a model may not predict accurately where exactly the peak around the 10 nm width may lie; however, one can make the qualitative deduction that an engineer of QD arrays for IBSCs should not make the QD so small as to make the lh(2,1,1) state disappear. It should be observed that the disappearance of the IB(2,1,1) and IB(2,2,1) states (dashed and dotted lines) corresponds to a decrease in the overall photocurrent received by the IB; however, the disappearance of these states is desirable from the point of view of maintaining a high

open-circuit voltage, as has been discussed in previous work. Further studies are required to identify the overall optimum configuration in this respect.

Despite a relative enhancement of around 2.5 between the peak in $j_{ph,VB\rightarrow IB(1,1,1)}^{max}$ at 10 nm and the benchmark value at 16 nm, the absorbed photocurrent remains extremely low. To achieve a viable QD-IBSC, significant further absorption enhancements will be necessary, perhaps through increasing the number of QD layers and/or photon management techniques.

IV. CONCLUSIONS

In summary, reduction of the QD width will increase the IB ground state absorption if the fractional surface coverage is conserved. Careful engineering is necessary for optimising this effect, i.e., taking care that certain states in the VB do not disappear. This adds to the number of possibilities for increasing the QD density that may lead to improved IB current, such as increasing the fractional QD coverage by, e.g., using higher index substrates,[22] and increasing the number of QD layers.

This work has been supported by the EC through the project NGCPV (Grant No. 283798) and the Comunidad de Madrid through the project NUMANCIA2 (Grant No. S2009/ENE1477). Alexander Mellor gratefully acknowledges the Comunidad de Madrid for financial support through the scholarship Personal Investigador de Apoyo.

[1] A. Luque and A. Martí, Physical Review Letters **78**, 5014–5017 (1997).
[2] W. Shockley and H. J. Queisser, Journal of Applied Physics **32**, 510–519 (1961).
[3] A. Luque, A. Marti, C. Stanley, N. Lopez, L. Cuadra, D. Zhou, J. L. Pearson, and A. McKee, Journal of Applied Physics **96**, 903–909 (2004).
[4] S. M. Hubbard, C. D. Cress, C. G. Bailey, R. P. Raffaelle, S. G. Bailey, and D. M. Wilt, Applied Physics Letters **92**, 123512–3 (2008).
[5] V. Popescu, G. Bester, M. C. Hanna, A. G. Norman, and A. Zunger, Physical Review B **78**, 205321 (2008).
[6] S. Blokhin, A. Sakharov, A. Nadtochy, A. Pauysov, M. Maximov, N. Ledentsov, A. Kovsh, S. Mikhrin, V. Lantratov, S. Mintairov, N. Kaluzhniy, and M. Shvarts, Semiconductors **43**, 514–518 (2009).
[7] R. Oshima, A. Takata, and Y. Okada, Applied Physics Letters **93**, 083111–3 (2008).
[8] C. G. Bailey, D. V. Forbes, R. P. Raffaelle, and S. M. Hubbard, in *Photovoltaic Specialists Conference (PVSC), 2011 37th IEEE*, Seattle, WA, USA, 2011, p. 003498–003498.
[9] A. Luque, A. Marti, N. Lopez, E. Antolin, E. Canovas, C. Stanley, C. Farmer, L. J. Caballero, L. Cuadra, and J. L. Balenzategui, Applied Physics Letters **87**, 083505–3 (2005).
[10] A. Martí, E. Antolín, C. R. Stanley, C. D. Farmer, N. López, P. Díaz, E. Cánovas, P. G. Linares, and A. Luque, Physical Review Letters **97**, 247701 (2006).
[11] A. Martí, C. R. Stanley, and A. Luque, in *Nanostructured Materials for Solar Energy Conversion*, edited by T. Soga (Elsevier Science, Amsterdam, 2006).
[12] E. Antolin, A. Marti, C. D. Farmer, P. G. Linares, E. Hernandez, A. M. Sanchez, T. Ben, S. I. Molina, C. R. Stanley, and A. Luque, Journal of Applied Physics **108**, 064513–7 (2010).
[13] A. Luque, A. Marti, E. Antolin, and P. Garcia-Linares, Solar Energy Materials and Solar Cells **94**, 2032–2035 (2010).
[14] A. Luque, A. Martí, A. Mellor, D. Fuertes Marrón, I. Tobías, and E. Antolín, "Absorption coefficient for the intraband transitions in quantum dot materials," Prog. Photovoltaics (in press).
[15] A. Luque, A. Martí, E. Antolín, P. G. Linares, I. Tobías, I. Ramiro, and E. Hernandez, Solar Energy Materials and Solar Cells **95**, 2095–2101 (2011).
[16] A. Luque, A. Mellor, E. Antolín, P. G. Linares, I. Ramiro, I. Tobías, and A. Martí, Solar Energy Materials and Solar Cells **103**, 171–183 (2012).
[17] A. Mellor, A. Luque, I. Tobias, and A. Marti, Applied Physics Letters **101**, 133909–4 (2012).
[18] A. Luque, A. Marti, E. Antolin, P. G. Linares, I. Tobias, and I. Ramiro, AIP Advances **1**, 022125–6 (2011).
[19] E. Antolin, A. Marti, P. G. Linares, I. Ramiro, E. Hernandez, C. D. Farmer, C. R. Stanley, and A. Luque, in *35th IEEE Photovoltaic Specialists Conference (PVSC) Honolulu*, HI, USA (2010), p. 000065–000070.
[20] S. Datta, *Quantum Phenomena*, Vol. VII (Addison-Wesley, Reading, Massachusetts, 1989).
[21] S. Tomic, T. S. Jones, and N. M. Harrison, Applied Physics Letters **93**, 263105–3 (2008).
[22] K. Akahane, T. Kawamura, K. Okino, H. Koyama, S. Lan, Y. Okada, M. Kawabe, and M. Tosa, Applied Physics Letters **73**, 3411–3413 (1998).